

A smooth polynomial shaped command for sloshing suppression of a suspended liquid container

Transactions of the Institute of
Measurement and Control
2021, Vol. 43(2) 278–294
© The Author(s) 2020
Article reuse guidelines:
sagepub.com/journals-permissions
DOI: 10.1177/0142331220949304
journals.sagepub.com/home/tim



Abdullah Alshaya  and Dima Almujaarab

Abstract

A smooth polynomial shaped command with an adjustable command time length is proposed for eliminating the residual vibrations of a multi-mode system. The ability of eliminating jerks and vibrational modes, regardless of their number, offers the most advantage of the proposed command. A numerical simulation is conducted to test the command's effectiveness by eliminating the residual sloshing oscillations of a liquid-filled container conveyed by an overhead crane in a rest-to-rest manoeuvre. The governing equations of the liquid free-surface level are derived by modelling the sloshing dynamics by a series of mass–spring–damper harmonics. The proposed model accounts for the coupling between the pendulum dynamics and the sloshing equivalent mechanical model. The command's robustness to the system parameters' uncertainties, liquid depth and cable length, are investigated as well. The ability of adjusting the command length and retaining higher sloshing modes in command-designing are also outlined.

Keywords

Sloshing suppression, command-shaping, overhead crane, open-loop control, vibration control

Introduction

In modern industrial automation systems, rest-to-rest manoeuvres, such as in robotic manipulators, overhead or gantry cranes, and automotive and space industries, are extensively used to convey containers between different locations. Such manoeuvres are functioned along automated lines and repeated cycles. Vibration control is usually employed to enhance the accuracy of manoeuvres and to lead to faster, safer, and cost-effective operations. In the case of conveying a liquid container subjected to rapid excitation, the problem of sloshing arises. The induced liquid sloshing may affect the motion stability which could cause accidents that compromise safety, result in an economic loss, delay the overall process, and cause structural fatigue from the long-term pressure on the container wall. Excessive liquid sloshing may also cause spillage (molten metal in the case of metal industries).

Two types of induced oscillations are experienced when conveying suspended liquid-filled containers: the sloshing of the liquid inside; and the swing motion of the overhead crane. Conveying the container at low speeds, often lower than the capability of driven-motors, limits its sway motion, and hence maintains sloshing within tolerable limits but incurs increasing operational time. Furthermore, considerable time is wasted while waiting for the residual vibrations to die out before issuing the next command. Lowering transient liquid sloshing reduces the risks of operations in conveying hazardous liquids, while lowering residual sloshing makes the operation efficient, fast and accurate. Therefore, to eliminate the induced transient and residual sloshing while reducing the operational time and ensuring a safe and cost-effective operation, a controlling technique has to be employed.

Recently, passive and active controlling techniques were extensively used by many researchers in controlling and suppressing the induced liquid sloshing. Even though adding absorbers and baffles as passive controlling techniques dissipates sloshing, it increases both the overall system's weight and complexity (Hasheminejad et al., 2014; Wang et al., 2016). Alternatively, active control techniques succeeded in suppressing liquid sloshing. Kaneshige et al. (1996, 1997) were among the first to use control systems to suppress liquid sloshing in overhead crane systems. Feddema et al. (1997) used the fundamental mode of oscillation and the damping of the liquid in an open container carried by a robot arm for controlling the surface of the liquid using an infinite impulse response filter. Yano and Terashima (2001) employed H^∞ control theory to suppress sloshing in transferring a liquid container horizontally and with the rotational motion of the container by modelling the sloshing dynamics as an equivalent simple pendulum. Kaneshige et al. (2009) proposed an autonomous mobile overhead crane system that detects obstacles and suppresses sloshing in the transfer of a liquid tank. Zang and Huang (2015) and Huang and Zhao (2018) developed a three-dimensional nonlinear slosh model for suppressing the sloshing in a moving container. Cooker

Mechanical Engineering Department, College of Engineering and Petroleum, Kuwait University, Safat, Kuwait

Corresponding author:

Abdullah Alshaya, Mechanical Engineering Department, College of Engineering and Petroleum, Kuwait University, PO Box 5969, Safat 13060, Kuwait.

Email: abdullah.alshaya@ku.edu.kw

(1994) modelled the induced wave motions in a suspended container. Turner and Bridges (2013) and Turner et al. (2015a, 2015b) derived the nonlinear equations of the free-surface motions for a suspended liquid-filled container. Several active control techniques which are proposed, simulated, and tested in sloshing suppression are given in Kaneshige et al. (2008), Reyhanoglu and Rubio Hervas (2013), Baozeng and Lemei (2014), Zang et al. (2015), and Biagiotti et al. (2018).

Unlike feedback control that requires liquid-motion sensors to acquire real-time measurements of the liquid sloshing, input shaping technique induces minimal transient and residual vibrations with a specially shaped input generated by convolving a general reference command signal with sequences of specified timed impulses. Singer and Seering (1990), Hyde and Seering (1991), Singer and Seering (1992), Singhose et al. (1994, 1996), and Singhose and Pao (1997) are among the first who used input shaping techniques to attenuate residual vibrations in different vibrational systems. The drawbacks of input shaping are the high sensitivity to modelling errors and parameter variations. Aboel-Hassan et al. (2009) and Zang et al. (2015) suppressed sloshing in moving containers using robust input shaping. Murthy et al. (2012) and AlSaibie and Singhose (2013) tested different input shaping methods in suppressing sloshing of a suspended liquid-filled container. Pridgen et al. (2013) designed multi-mode robust input shapers for slosh suppression in a laterally moving liquid-filled container. Xing and Huang (2020) recently suppressed the liquid sloshing in a suspended container by designing a smooth robust shaper that targets the fundamental mode and attenuates the higher modes by means of low-pass filtration.

Using a single-mode control that targets the induced vibrations from the primary mode while neglecting the higher modes does not guarantee complete elimination of the residual vibrations. Since the sloshing can be modelled as a multidegree-of-freedom system, this necessitates the use of a multi-mode command controller. Alhazza and Masoud (2016), Masoud and Alhazza (2017), and Alshaya and Alghanim (2020) proposed a multi-steps input command and a waveform command to eliminate the residual vibrations of multi-mode systems. Alghanim et al. (2018) proposed a polynomial-based command for a single degree-of-freedom system. Unlike multi-steps input commands which usually degrade the performance due to actuation delay and mismatch timing, reduce the life expectancy of the actuator, and increase maintenance due to jerks, the continuous form of the polynomial-based command can be easily adjusted to have any level of smoothness. The aim of this work is to propose a smooth polynomial shaped command (PSC) that produces fast manoeuvring and accurate positioning while eliminating the residual vibrations of all the modes in a multi-mode system. The proposed command is utilized to suppress all the sloshing modes induced from conveying a suspended liquid container by an overhead crane with different design and system parameters. The derived model in this work is based on modelling the sloshing dynamics as a series of mass-spring-damper systems and it accounts for the coupling between the pendulum dynamics from the overhead crane and the sloshing equivalent mechanical model.

Designing a PSC

In this section, a PSC is proposed to eliminate the excited vibrations of a multi-mode system leading to zero residual vibrations at the end of the command duration. The specific rest-to-rest manoeuvre conditions are also outlined.

Theoretical development

A multi-mode linear system of order N with a single input can be generally written as in Equation (1):

$$\mathbf{M}\ddot{\Theta}(t) + \mathbf{C}\dot{\Theta}(t) + \mathbf{K}\Theta(t) = \mathbf{B}f(t) \quad (1)$$

where \mathbf{M} , \mathbf{C} , and \mathbf{K} are the mass, damping, and stiffness matrices, Θ is the generalized coordinates vector, \mathbf{B} is a constant vector, and $f(t)$ is the system single input. The natural frequencies of the undamped system, $\omega_{n,i}$ and their corresponding mode shapes, Φ_i , can be obtained from the characteristic equation, Equation (2):

$$(\mathbf{K} - \omega_{n,i}^2 \mathbf{M})\Phi_i = \mathbf{0}, \quad \text{for } i = 1, 2, \dots, N \quad (2)$$

where $\Phi = [\Phi_1 \ \Phi_2 \ \dots \ \Phi_N]^T$ is the modal matrix where each of its columns represents the normal mode corresponding to $\omega_{n,i}$. The system of Equation (1) can be further decoupled using modal analysis by expressing the generalized coordinates $\Theta(t)$ in terms of the mode shapes as given by Equation (3):

$$\Theta(t) = \Phi\Psi(t) = \sum_{i=1}^N \Phi_i\psi_i(t) \quad (3)$$

where $\Psi(t) = \{\psi_1(t) \ \psi_2(t) \ \dots \ \psi_N(t)\}^T$ is the time-dependent generalized principal (decoupled) coordinates vector. Upon carrying the first and second derivatives of Equation (3) and substituting the results into Equation (1) and then pre-multiplying the resultant equation by Φ^T to utilize the orthogonality property of the mode shapes, the equations of motion are given by Equation (4):

$$m_i\ddot{\psi}_i + c_i\dot{\psi}_i + k_i\psi_i = p_i f(t), \quad \text{for } i = 1, 2, \dots, N \quad (4)$$

where m_i , c_i , and k_i are the diagonal elements of the diagonal matrices $\mathbf{m} = \Phi^T \mathbf{M} \Phi$, $\mathbf{c} = \Phi^T \mathbf{C} \Phi$, and $\mathbf{k} = \Phi^T \mathbf{K} \Phi$, respectively, and p_i are the elements of the vector $\mathbf{p} = \Phi^T \mathbf{B}$. It should be noted that the damping matrix, \mathbf{C} , has to be linearly proportional to the mass and stiffness matrices, otherwise the modal damping matrix, \mathbf{c} , will not be fully uncoupled.

Polynomial Shaped Command (PSC)

A general polynomial profile of order m^1 is proposed, as given by Equation (5):

$$\ddot{u}(t) = \sum_{k=0}^m a_k t^k \quad (5)$$

where a_k are the polynomial coefficients. Substitution of Equation (5) into Equation (4) and assuming all the principal coordinates experience underdamped vibration, that is, $\zeta_i < 1$ and zero initial conditions, the general solutions of $\psi_i(t)$ and their time derivatives using Duhamel integral are given by Equations (6) and (7):

$$\psi_i(t) = \left[1 - e^{-\zeta_i \omega_{n,i} t} \left(\cos \omega_{d,i} t + \frac{\zeta_i \omega_{n,i}}{\omega_{d,i}} \sin \omega_{d,i} t \right) \right] b_{i,0} + \left[t - \frac{1}{\omega_{d,i}} e^{-\zeta_i \omega_{n,i} t} \sin \omega_{d,i} t \right] b_{i,1} + \sum_{k=2}^m b_{i,k} t^k \quad (6)$$

$$\dot{\psi}_i(t) = \left[\frac{\omega_{n,i}^2}{\omega_{d,i}} e^{-\zeta_i \omega_{n,i} t} \sin \omega_{d,i} t \right] b_{i,0} + \left[1 + \frac{e^{-\zeta_i \omega_{n,i} t}}{\omega_{d,i}} (\zeta_i \omega_{n,i} \sin \omega_{d,i} t - \omega_{d,i} \cos \omega_{d,i} t) \right] b_{i,1} + \sum_{k=2}^m k b_{i,k} t^{k-1} \quad (7)$$

where $\omega_{n,i} = \sqrt{k_i/m_i}$ and $\omega_{d,i} = \omega_{n,i} \sqrt{1 - \zeta_i^2}$ are the undamped and damped natural frequencies of the multi-mode system, respectively. The coefficients $b_{i,k}$ are defined by the following recursive relations, as given by Equation (8):

$$\begin{aligned} b_{i,m} &= \frac{p_i a_m}{k_i} \\ b_{i,m-1} &= \frac{p_i a_{m-1} - m c_i b_{i,m}}{k_i} \\ b_{i,k} &= \frac{p_i a_k - (k+1) c_i b_{i,k+1} - (k+1)(k+2) m_i b_{i,k+2}}{k_i} \end{aligned} \quad (8)$$

for $k = m-2, m-3, \dots, 1, 0$

If one of the principal coordinates experiences critical or overdamped vibration, Equations (6) and (7) should be adjusted accordingly. The recursive relations in Equation (8) can be written in a matrix form as $\mathbf{T}_i \mathbf{b}_i = p_i \mathbf{a}$ where $\mathbf{b}_i = \{b_{i,0} \ b_{i,1} \ \dots \ b_{i,m}\}^T$, $\mathbf{a} = \{a_0 \ a_1 \ \dots \ a_m\}^T$ and \mathbf{T}_i is a tri-diagonal square matrix, namely, as given by Equation (9):

$$\begin{bmatrix} k_i & c_i & 2m_i & 0 & \dots & 0 & 0 & 0 \\ 0 & k_i & 2c_i & (3)(2)m_i & \dots & 0 & 0 & 0 \\ 0 & 0 & k_i & 3c_i & \dots & 0 & 0 & 0 \\ \vdots & \vdots & \vdots & \vdots & \ddots & \vdots & \vdots & \vdots \\ 0 & 0 & 0 & \dots & \dots & k_i & (m-1)c_i & m(m-1)m_i \\ 0 & 0 & 0 & \dots & \dots & 0 & k_i & m c_i \\ 0 & 0 & 0 & \dots & \dots & 0 & 0 & k_i \end{bmatrix} \begin{bmatrix} b_{i,0} \\ b_{i,1} \\ b_{i,2} \\ \vdots \\ b_{i,m-2} \\ b_{i,m-1} \\ b_{i,m} \end{bmatrix} = p_i \begin{bmatrix} a_0 \\ a_1 \\ a_2 \\ \vdots \\ a_{m-2} \\ a_{m-1} \\ a_m \end{bmatrix} \quad (9)$$

The polynomial coefficients, a_k , must be determined by satisfying zero residual vibrations at the end of the command duration. If the time interval of the shaped command is chosen to be τ , then substitution of $t = \tau$ into the solution of the principal coordinates ψ_i , Equation (6), and its time derivatives, Equation (7), yields a system of linear algebraic equations (Equations (10) to (12)):

$$\mathbf{A}_i \mathbf{b}_i = \mathbf{0} \quad (10)$$

where \mathbf{A}_i is a matrix of size $2 \times (m+1)$ and its elements are defined as,

$$\begin{aligned} \mathbf{A}_i(1,1) &= 1 - e^{-\zeta_i \omega_{n,i} \tau} \left(\cos \omega_{d,i} \tau + \frac{\zeta_i \omega_{n,i}}{\omega_{d,i}} \sin \omega_{d,i} \tau \right) \\ \mathbf{A}_i(1,2) &= \tau - \frac{1}{\omega_{d,i}} e^{-\zeta_i \omega_{n,i} \tau} \sin \omega_{d,i} \tau \\ \mathbf{A}_i(1,k) &= \tau^{k-1} \\ \mathbf{A}_i(2,1) &= \frac{\omega_{n,i}^2}{\omega_{d,i}} e^{-\zeta_i \omega_{n,i} \tau} \sin \omega_{d,i} \tau \\ \mathbf{A}_i(2,2) &= 1 + \frac{e^{-\zeta_i \omega_{n,i} \tau}}{\omega_{d,i}} (\zeta_i \omega_{n,i} \sin \omega_{d,i} \tau - \omega_{d,i} \cos \omega_{d,i} \tau) \\ \mathbf{A}_i(2,k) &= (k-1) \tau^{k-2} \text{ for } k = 3, 4, \dots, 2N \end{aligned} \quad (11)$$

Upon using $\mathbf{b}_i = p_i \mathbf{T}_i^{-1} \mathbf{a}$ from Equation (9), one can rewrite Equation (10) in terms of the polynomial coefficients, $\mathbf{a} = a_k$, as given by Equation (12):

$$\mathbf{U} \mathbf{a} = \mathbf{0} \quad (12)$$

where matrix $\mathbf{U} = p_i \mathbf{A}_i \mathbf{T}_i^{-1}$ has a size of $2N \times (m+1)$. For a system with negligible damping (undamped), Equation (12) can be used by setting $\zeta_i = 0$ in Equation (11). Additional physical constraints on the system input command such as maximum velocity, force and/or power have to be imposed to have a nontrivial solution. The only information needed are the natural frequencies and damping ratios of the multi-mode system to design the PSC where its duration is adjustable and independent of the system frequencies and damping ratios. However, decreasing the manoeuvre time will increase the sensitivity of the system and will consequently affect the command performance. The mathematical analysis of the PSC can be successfully applied on many systems such as cranes conveying multi-loads or liquid containers and translating or rotating beams.

Problem formulation

The effectiveness of the proposed PSC is tested by suppressing the induced residual liquid sloshing by an overhead crane conveying a rigid-walled liquid-filled container as shown in Figure 1(a). The overhead crane is modelled by a moving jib (slider) with a proposed predefined acceleration command, $\ddot{u}(t)$, while the rigid-walled container of mass m_c , width W , and height H swings in the xy -plane with an oscillation angle $\theta(t)$. The container has a mass moment of inertia I_c with respect to its own centre of mass. It is filled with water of a

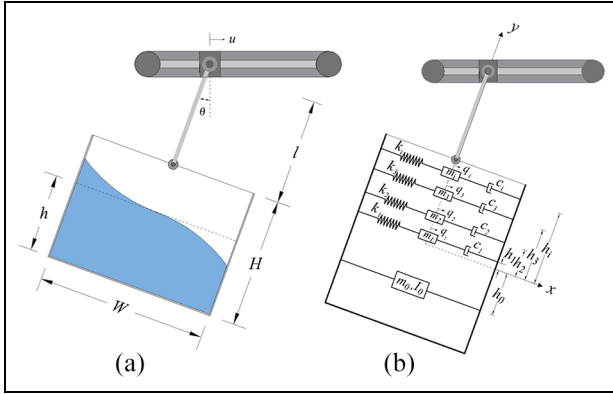


Figure 1. (a) a rigid-walled liquid-filled container conveyed by an overhead crane; and (b) the corresponding equivalent mechanical model of the liquid sloshing modes.

filling level h and attached to the sliding jib by a rigid massless link of length l .

Mechanical model of sloshing dynamics

Figure 1(b) shows the corresponding equivalent mass–spring–damper mechanical system that each represents one of the vibratory modes of the liquid sloshing. The sloshing dynamics of this equivalent mechanical model are the same as multiple pendulum systems. Even though the dynamics behaviour of the sloshing induced by the combination of heaving and pitching excitations is generally nonlinear, this equivalent mechanical model provides a realistic representation of the liquid free-surface wave oscillations as stated in Graham and Rodriguez (1952) and Ibrahim (2005). For simplicity, only the lateral motion is considered.

The liquid inside the container can be modelled as two parts: a fixed part moving with the container; and the other part induces the sloshing waves. The fixed part is modelled as a rigidly attached mass, m_0 , and a moment of inertia I_0 (see Figure 1(b)). The liquid which experiences sloshing is represented by a series of n lumped (point) masses, m_i , attached to the container’s walls by an equivalent spring stiffness k_i and equivalent viscous damper c_i ($i = 1, 2, \dots, n$) (see Figure 1(b)). The corresponding motion of the liquid surface of the i -th sloshing mode is represented by the relative displacement q_i of mass m_i with respect to the container’s walls along the container-fixed lateral axis. The distances from the liquid centre of mass in its undistributed condition, $h/2$, to the the rigid mass, m_0 , and the equivalent i -th lumped mass, m_i are denoted by h_0 and h_i , respectively. The container’s shape and dimension and liquid’s filling depth, h , and characteristic define the values of $m_0, I_0, h_0, m_i, h_i, k_i, c_i$ of the equivalent mechanical system as given in Graham and Rodriguez (1952) and Ibrahim (2005).

The liquid free-surface elevation is given by Equation (13):

$$\eta(x, y, t) = \sum_{i=1}^n \phi_i(x, y)q_i(t) \quad (13)$$

where $\phi_i(x, y)$ is the i -th sloshing spatial mode function and $q_i(t)$ is the time-dependent function. The surface wave motion at the edges of the container ($x = \pm W/2$ and $y = 0$), where the spillage is most likely to occur, is given by Equation (14):

$$\delta(t) = \eta(\pm W/2, 0, t) = \sum_{i=1}^n \phi_i(\pm W/2, 0)q_i(t) \quad (14)$$

Mathematical model

The position vectors of the container’s centre of mass, the liquid fixed-mass, m_0 , and the i -th point mass, m_i are given, respectively, by Equations (15) to (17):

$$\mathbf{P}_c = [u - l_c \sin \theta, -l_c \cos \theta] \quad (15)$$

$$\mathbf{P}_0 = [u - l_0 \sin \theta, -l_0 \cos \theta] \quad (16)$$

$$\mathbf{P}_i = [u - l_i \sin \theta + q_i \cos \theta, -l_i \cos \theta - q_i \sin \theta] \quad (17)$$

for $i = 1, 2, \dots, n$

where u is the jib horizontal displacement and $l_c = l + H/2$, $l_0 = l + H - h/2 + h_0$, and $l_i = l + H - h/2 - h_i$ are the distances from the jib to the container’s centre of mass, the liquid fixed-mass, m_0 , and the i -th lumped mass, m_i , respectively. Upon using Lagrange’s formulation, the following fully coupled nonlinear differential equations (Equations (18a), (18b), (19a) and (19b)) in the angular coordinate $\theta(t)$ and the n lateral relative displacements $q_i(t)$ were obtained:

$$\begin{aligned} & \left[I_{eq} + \sum_{i=1}^n m_i q_i^2 \right] \ddot{\theta} - \sum_{i=1}^n m_i l_i \ddot{q}_i + 2 \left[\sum_{i=1}^n m_i q_i \dot{q}_i \right] \dot{\theta} \\ & + \left[M_l g - \ddot{u} \sum_{i=1}^n m_i q_i \right] \sin \theta \\ & - \left[\sum_{i=1}^n m_i q_i \right] g \cos \theta = M_l \ddot{u} \cos \theta \end{aligned} \quad (18a)$$

$$\begin{aligned} m_i \ddot{q}_i + 2\zeta \omega_i m_i \dot{q}_i + (\omega_i^2 - \dot{\theta}^2) m_i q_i - m_i l_i \ddot{\theta} - m_i g \sin \theta \\ = -m_i \ddot{u} \cos \theta \quad \text{for } i = 1, 2, \dots, n \end{aligned} \quad (18b)$$

where ω_i and ζ are the natural frequency of the mass-spring-damper systems and liquid damping ratio, respectively, g is the gravitational acceleration, and

$$I_{eq} = I_c + m_c l_c^2 + I_0 + m_0 l_0^2 + \sum_{i=1}^n m_i l_i^2 \quad \text{and}$$

$$M_l = m_c l_c + m_0 l_0 + \sum_{i=1}^n m_i l_i$$

Assuming small oscillations of angle θ and surface wave motion q_i and neglecting higher order terms, Equations (18a) and (18b) are reduced to Equations (19a) and (19b):

$$I_{eq} \ddot{\theta} - \sum_{i=1}^n m_i l_i \ddot{q}_i + M_l g \theta - g \sum_{i=1}^n m_i q_i = M_l \ddot{u} \quad (19a)$$

$$\begin{aligned} -m_i l_i \ddot{\theta} + m_i \ddot{q}_i + 2\zeta \omega_i m_i \dot{q}_i - m_i g \theta + \omega_i^2 m_i q_i \\ = -m_i \ddot{u} \quad \text{for } i = 1, 2, \dots, n \end{aligned} \quad (19b)$$

Equations (19a) and (19b) can be written in a matrix form as in Equation (1) with generalized coordinates given by $\Theta = \{\theta \ q_1 \ \dots \ q_n\}^T$ and the jib acceleration as the system input, $f(t) = \ddot{u}(t)$.

Command designing

The absence of the system's natural frequencies and the presence of nonlinearities in Equations (18a) and (18b) necessitates the need of using the linearized Equations (19a) and (19b) when designing the PSC. The basic operation of the rest-to-rest manoeuvres consist of three stages: acceleration; cruising; and deceleration. It is practical to dissipate the induced residual vibrations before the next stage is introduced. For subsequent analysis, the time lengths of the acceleration, cruising, and deceleration stages are denoted by t_a , t_c , and t_d , respectively.

To have zero residuals at the end of the command interval, $\delta(t)$ and $\theta(t)$ and their time derivatives have to be set to zero. Furthermore, to achieve an optimum manoeuvre time, $T = t_a + t_c + t_d$, the command should utilize the full input velocity, v_f , and acceleration, a_{\max} , capabilities. Therefore, the following constraints during the acceleration stage have to be imposed, as given by Equation (20):

$$\begin{aligned} \theta(t_a) = 0, \quad \dot{\theta}(t_a) = 0, \quad \delta(t_a) = 0, \quad \dot{\delta}(t_a) = 0, \\ \int_0^{t_a} \ddot{u}(t) dt = v_f, \quad |\ddot{u}| \leq a_{\max} \end{aligned} \quad (20)$$

The wave motion amplitude of the free-surface $\delta(t_a)$ will equal zero if $q_i(t_a) = 0$ for all values of i as suggested from Equation (14). The equality constraints in Equation (20) produce $2(n+1) + 1 = 2n + 3$ equations. Therefore, at least $2n + 3$ coefficients, that is, a polynomial of order $m = 2n + 2$, are needed to satisfy all the equality constraints in Equation (20) while ensuring that $|\ddot{u}| < a_{\max}$.

According to Equation (3), the swing angle and the liquid wave surface motion will be zero at the end of the acceleration stage, $t = t_a$, if all the principal coordinates, ψ_i , (for $i = 1, 2, \dots, N$ where N in this case is $N = n + 1$) are set to zero at $\tau = t_a$. To ensure that the jib reaches its maximum velocity, Equation (5) should be integrated from 0 to t_a and equated to the required cruising speed v_f , namely, as given by Equation (21):

$$\int_0^{t_a} \ddot{u}(t) dt = \sum_{k=0}^m \frac{a_k}{k+1} t_a^{k+1} = v_f \quad (21)$$

Upon combining Equations (20) and (21) with Equation (12), one can simultaneously solve for the polynomial coefficients, a_k . The shaper that satisfies the specific rest-to-rest manoeuvre conditions, Equation (20), is referred to herein as an *unsmooth* shaper.

The sudden movement of the jib at the beginning and the end of the acceleration and deceleration stages may affect the motor's performance. Therefore, additional constraints of

zero acceleration at the beginning and the end of the acceleration (and deceleration) stages can be imposed, as given by Equation (22):

$$\ddot{u}(0) = 0, \quad \ddot{u}(t_a) = 0 \quad (22)$$

To satisfy this condition, two more polynomial coefficients should be added which gives a total of $2n + 5$ coefficients. The shaper that satisfies the rest-to-rest constraints, Equation (20), and zero initial and final acceleration in the acceleration (and deceleration) stage, Equation (22), is referred to as a *semi-smooth* shaper.

Furthermore, the smoothness of the command profile at the beginning and the end of the acceleration (and deceleration) stage can also be enhanced by forcing the jerk to be zero at $t = 0$ and t_a , that is, as given by Equation (23):

$$\dddot{u}(0) = 0, \quad \dddot{u}(t_a) = 0 \quad (23)$$

Therefore, the shaper with $2n + 7$ coefficients that satisfies the essential rest-to-rest constraints, Equation (20), and zero acceleration and jerk at the beginning and end of the acceleration (and deceleration) stage, Equations (22) and (23), is referred to as a *smooth* shaper.

In order to bring the slider to a complete stop at the target point, the magnitudes of the polynomial coefficients in the deceleration stage are basically the inversion of those in the acceleration stage. The covered distance during either the acceleration, s_a , or deceleration, s_d , stages are determined as given by Equation (24):

$$s_a = s_d = \int_0^{t_a} \int_0^{\hat{t}} \ddot{u}(t) dt d\hat{t} = \sum_{k=0}^m \frac{a_k}{(k+1)(k+1)} t_a^{k+2} \quad (24)$$

To ensure that the jib moves a certain travel distance, d , the covered distance during the cruising stage is $s_c = d - 2s_a$ and the corresponding time interval is $t_c = s_c/v_f$. Therefore, the deceleration command has to start at $t_a + t_c$.

Even though that the designing of the command is independent of the command's time length, τ , the latter is constrained by the maximum jib acceleration, a_{\max} , and the total travelling distance, d . In the case of a fast command (small time duration τ), the maximum acceleration of the PSC may exceed the predefined maximum acceleration, a_{\max} , and will result in higher sloshing waves. In contrast, for the case of a short manoeuvre distance or slow command (large time duration τ), the start time of the deceleration stage may fall within the acceleration phase. This implies that the shaped command does not utilize the maximum acceleration and/or velocity capabilities of the system.

Simulation results

When designing a PSC to suppress the liquid sloshing of the free-surface wave, two factors should be considered: how many sloshing modes have to be employed; and how deep is the liquid. Some applications require considering the higher modes and not only rely on the fundamental sloshing mode. The maximum jib velocity and acceleration, the total travelled distance, the dimensions of the container, and the properties

Table 1. Kinematics of the jib, dimensions of the container, and the properties of the liquid (water) used in numerical simulation.

Container dimensions	Value	Jib kinematics	Value
Width, W (cm)	25	Travel distance, d (m)	0.6
Height, H (cm)	50	Maximum velocity, v_f (m/s)	0.3
Cable length, l (cm)	30	Maximum acceleration, a_{max} (m/s^2)	0.9
Container properties		Liquid (water) parameters	
Mass, m_c (kg)	10	Mass density, ρ (kg/m^3)	1000
Mass moment of inertia, I_c ($kg \cdot m^2$)	0.01	Liquid filling level, h (cm)	2.5

Table 2. Comparison of natural frequencies in (rad/s) between the laterally excited system and the linearized suspended system for a liquid filling depth of $h/W = 0.1$ and cable length ratio of $l/H = 0.6$.

Lateral motion	Suspended system–Sloshing modes			
	Equation (26e)	Single	Three	Five
$\omega_0 = \sqrt{g/l_{eff}}$	3.9110	3.8282	3.8277	3.8277
ω_1	6.1239	7.5799	7.5584	7.5576
ω_2	16.502		17.094	17.091
ω_3	23.776		24.03	24.025
ω_4	29.017			29.138
ω_5	33.193			33.260

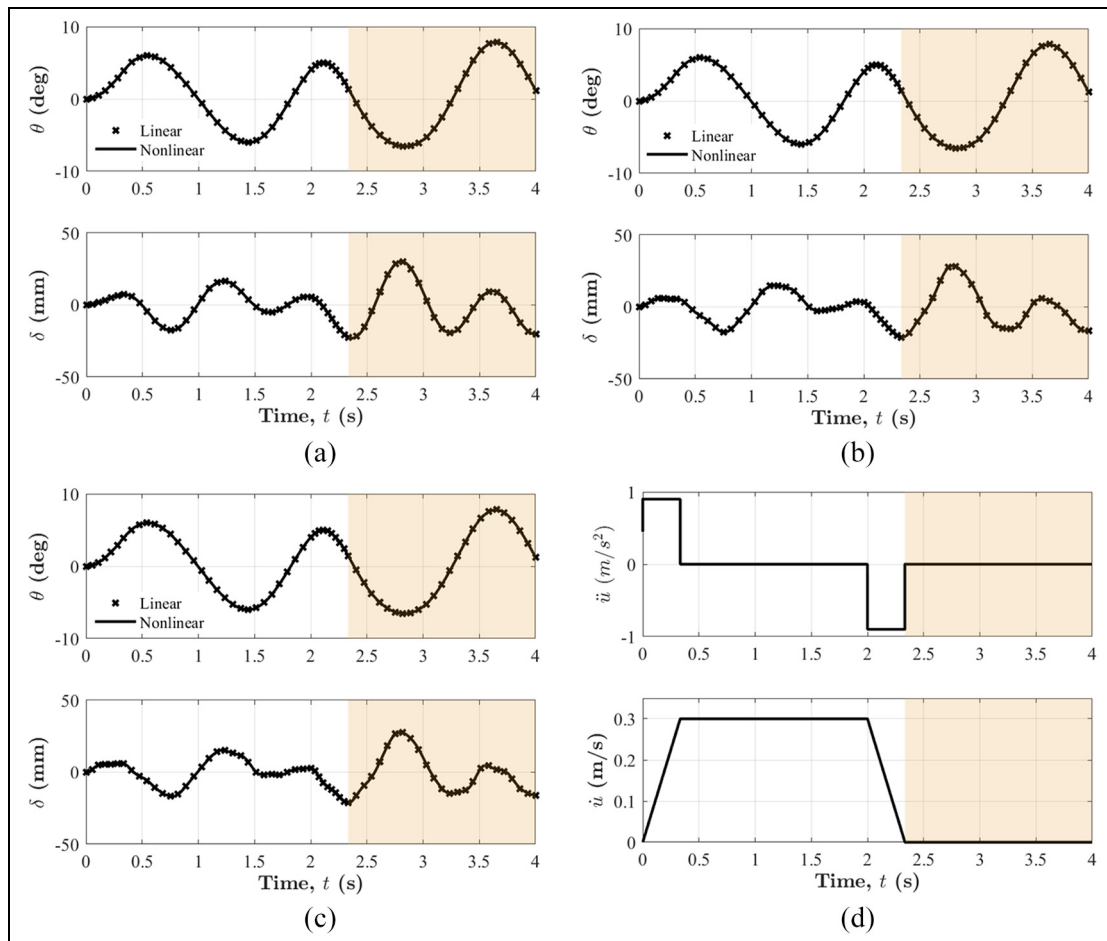


Figure 2. Time-optimal–rigid-body profile and corresponding dynamic transient (unshaded) and residual (shaded) responses using (a) single, (b) three, and (c) five sloshing modes, and (d) command profile ($h/W = 0.1$ and $l/H = 0.6$).

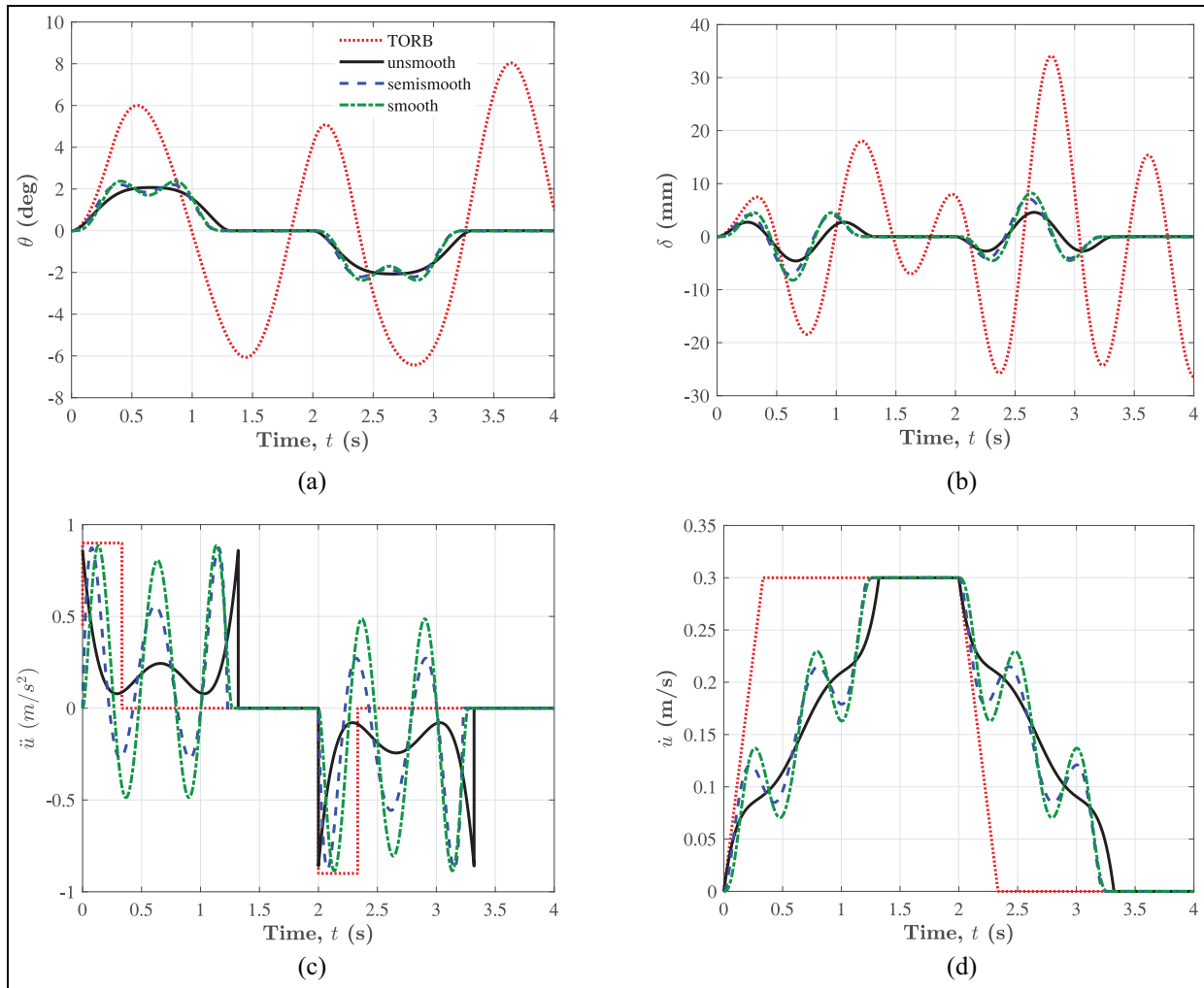


Figure 3. Different PSC profiles and their corresponding dynamic responses ($h/W = 0.1$, $l/H = 0.6$, $n = 1$, and the smallest manoeuvre time): (a) swing angle; (b) free-surface wave motion; (c) jib acceleration; and (d) jib velocity.

Table 3. Coefficients of different input polynomial profiles with the smallest manoeuvre time ($h/W = 0.1$, $l/H = 0.6$, and $n = 1$).

Case	a_0	a_1	a_2	a_3	a_4	a_5	a_6	a_7	a_8
Unsmooth	0.8596	-6.907	20.51	-23.15	8.769	-	-	-	-
Semismooth	0	26.82	-263.2	912.9	-1429	1032	-279.7	-	-
Smooth	0	0	239.7	-2321	8563	-15660	15170	-7466	1470

of the liquid (water) used in the numerical simulation are listed in Table 1. The Graham and Rodriguez (1952) model is utilized here to obtain the masses, spring constants, and damping constants of the sloshing modes as given in Equations (26a) to (26i) in the Appendix. The analyses are conducted by neglecting the damping effects which represents the worst-case scenario. The polynomial coefficients of the PSC, a_k , are determined from the linear resonant frequencies where the dynamics response is obtained from the nonlinear governing Equation (18).

Natural frequencies

The natural frequencies of the linearized suspended system can be determined from Equation (2) for different numbers of sloshing modes. The obtained natural frequencies from the current model agreed very well with those determined from a model proposed by Xing and Huang (2020). Two previous studies by Murthy et al. (2012) and AlSaibie and Singhose (2013) utilized Equation (26e) in the Appendix to determine the natural frequencies of the suspended container to design

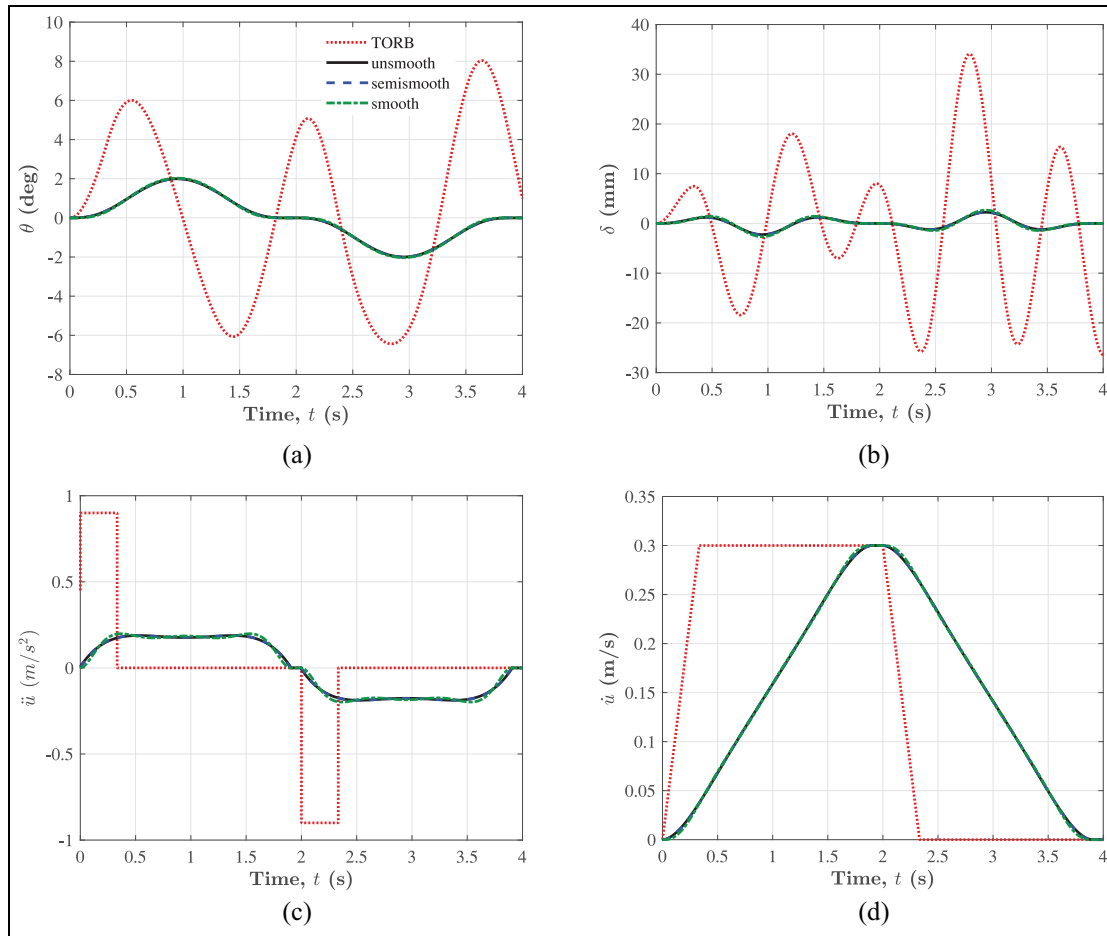


Figure 4. Different PSC profiles and their corresponding dynamic responses ($h/W = 0.1, l/H = 0.6, n = 1$ and a manoeuvre time of $T = 3.90$ s): (a) swing angle; (b) free-surface wave motion; (c) jib acceleration; and (d) jib velocity.

Table 4. The ranges of the acceptable manoeuvre time (in second) and their corresponding sloshing oscillation Q in (mm) for different SPC profiles ($h/W = 0.1$ and $l/H = 0.6$).

n	Unsmooth		Semismooth		Smooth	
	$[T_{min}, T_{max}]$	$[Q_{min}, Q_{max}]$	$[T_{min}, T_{max}]$	$[Q_{min}, Q_{max}]$	$[T_{min}, T_{max}]$	$[Q_{min}, Q_{max}]$
1	[3.32, 3.99]	[2.272, 1.036]	[3.23, 3.99]	[3.269, 0.938]	[3.27, 3.99]	[3.608, 1.048]
3	[3.26, 3.99]	[2.575, 1.043]	[3.28, 3.90]	[2.419, 0.938]	[3.35, 3.99]	[2.324, 1.288]
5	[3.35, 3.99]	[2.093, 1.184]	[3.28, 3.99]	[3.023, 1.238]	[3.29, 3.99]	[3.021, 1.259]
7	[3.22, 3.99]	[2.998, 1.222]	[3.27, 4.00]	[2.844, 1.468]	[3.45, 4.04]	[2.071, 1.477]

the input-shaping. The natural frequency of any suspended body can be approximated as $\omega_0 = \sqrt{g/l_{eff}}$ where l_{eff} is the effective length from the jib to the body’s centre of mass. It is worth noting that Equation (26e) in the Appendix was derived based on the assumption that the rectangular container was only excited in the lateral direction. Using the parameters given in Table 1, the approximated natural frequencies due to the swinging motion, ω_0 , and the laterally excited frequencies, ω_i , from Equation (26e) in the Appendix are listed in Table 2. However, the obtained natural frequencies that consider the swing motion of the liquid inside the suspended container

with single, three, and five sloshing modes obtained from Equation (2) are also listed in Table 2. It is worth noting that there is a 20% difference between the second natural frequency determined from Equation (2) with that determined from Equation (26e) in the Appendix.

Variation of system and command-designing parameters

For comparison, the time-optimal-rigid-body (TORB) command which represents the fastest possible command profile

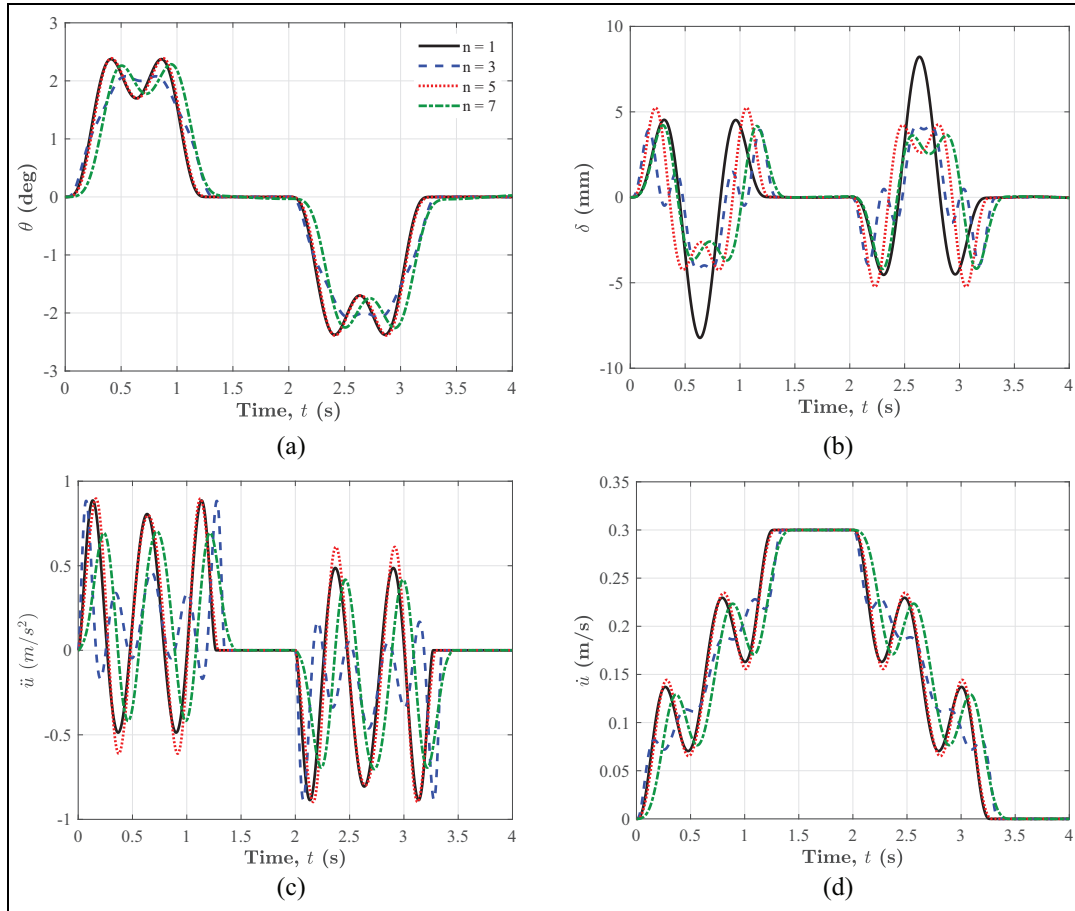


Figure 5. Smooth PSCs and the corresponding dynamic responses using different sloshing modes ($h/W = 0.1$ and $l/H = 0.6$): (a) swing angle; (b) free-surface wave motion; (c) jib acceleration; and (d) jib velocity.

based on utilizing the full input acceleration and velocity capabilities regardless of the output response is considered as the reference case of the uncontrolled (unshaped) command. The manoeuvre time of TORB is $T = 2.33$ s. The transient (unshaded) and residual (shaded) dynamics responses, $\theta(t)$ and $\delta(t)$, of TORB using the nonlinear equations of motion (Equation (18)), and the linearized form (Equation (19)), are illustrated in Figure 2 for different retained sloshing modes. The maximum swing angle is within the acceptable range of the linearity assumption which supports the use of the linear form in command-designing.

Variation of command length. For a single sloshing mode with liquid filling ratio of $h/W = 0.1$, the profiles of the unsmooth ($T = 3.32$ s), semismooth ($T = 3.23$ s) and smooth ($T = 3.27$ s) PSCs and their corresponding dynamics responses are illustrated in Figure 3. The corresponding coefficients of the PSCs for each of the unsmooth, semismooth and smooth profiles are listed in Table 3. Even though the unsmooth, semismooth, and smooth profiles make the system 42.3% (3.32 versus 2.33 s), 38.4% (3.23 versus 2.33 s), and 40.1% (3.27 versus 2.33 s) slower than TORB, the reduction

in the sloshing waves is significant (see Figure 3(b)). It is clear from Figures 3(c) and 3(d) that the PSCs utilize the maximum acceleration and velocity capabilities to achieve the optimum manoeuvre time. The semismooth and smooth profiles, and hence their dynamic responses, are almost similar. The profiles become smoother as the manoeuvre time increases, that is, making the system moves slowly, as shown in Figure 4 (corresponding to a manoeuvre time of $T = 3.90$ s). Even though the sloshing was significantly reduced, the system is 67.4% (3.90 versus 2.33 s) slower than the TORB.

The liquid inside the container, which is basically a continuous system, can be modelled by a sufficient large n multidegree-of-freedom systems. The input command designed based on a large number of lumped masses in the equivalent mechanical model will naturally give higher accuracy of the resulting sloshing dynamics. Using a time increment of 0.01 seconds that represents the sampling time of an actuator's hardware, the acceptable ranges of the manoeuvre times that are within $T \in [T_{\min}, T_{\max}]$, the designed PSC satisfies the rest-to-rest constraints for different numbers of sloshing modes are listed in Table 4. The root-mean-square of the amplitude oscillations of the free-surface wave,

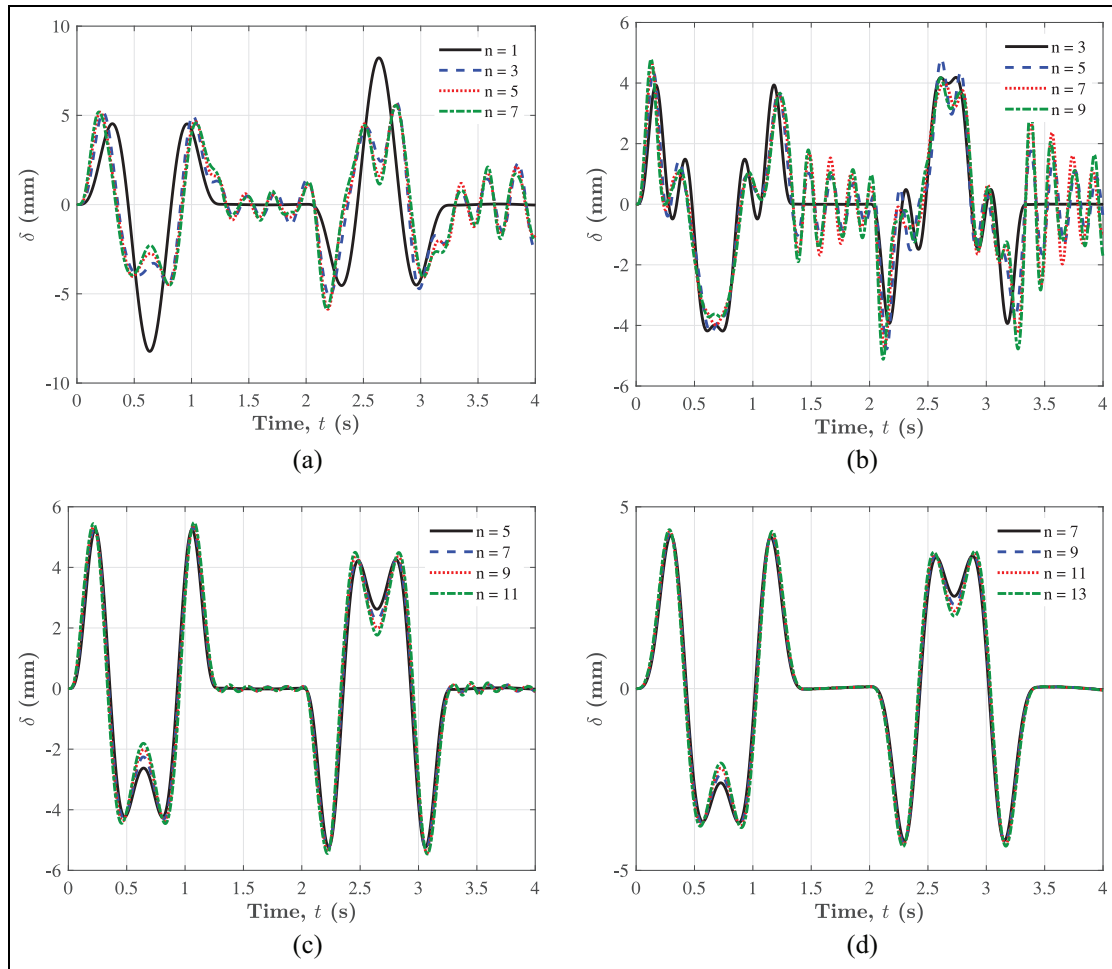


Figure 6. The free-surface wave motion when using higher sloshing modes with smooth PSC designed based on (a) 7, (b) 11, (c) 15, and (d) 19 polynomial coefficients ($h/W = 0.1$ and $l/H = 0.6$): (a) seven coefficients; (b) 11 coefficients; (c) 15 coefficients; and (d) 19 coefficients.

$$Q = \sqrt{\frac{\sum_{j=1}^m \left[\sum_{i=1}^n q_i(t_j) \right]^2}{m}}$$

is used to quantify the sloshing oscillation. The terms Q_{\min} and Q_{\max} , respectively, denote the sloshing oscillations corresponding to the smallest, T_{\min} and largest, T_{\max} manoeuvre time. It is clear from Table 4 that increasing the manoeuvre time will significantly reduce the sloshing oscillations. For instance, when using a single sloshing mode with $h/W = 0.1$, the response of the semismooth PSC reduces the sloshing oscillations by 71% (3.269 versus 0.938 mm) with the price of making the system 24% slower (3.23 versus 3.99 s). Furthermore, using the semismooth PSC will make the system faster than the unsmooth (3.23 versus 3.32 s) and the smooth (3.23 versus 3.27 s) commands and will result in a larger reduction in the sloshing oscillations, Q , compared to the unsmooth (0.938 versus 1.036 mm) and smooth (0.938 versus 1.048 mm) commands, respectively. Similar behaviour can be observed for higher sloshing modes. Therefore, it is recommended to use either the semismooth or the smooth

PSCs rather than using the unsmooth command to avoid the sudden movement of the jib at the beginning and the end of the acceleration and deceleration stages.

Retaining higher sloshing modes. The PSC designed based on a single sloshing mode has a high sensitivity in the variations of the modeling error and system parameters. Using a liquid depth ratio of $h/W = 0.1$ and cable length ratio of $l/H = 0.6$, the dynamic responses of the smooth PSC for different numbers of sloshing modes are illustrated in Figure 5. Considering the higher sloshing modes in command-designing necessitates the need for using higher polynomial orders of the shaped command and results in a larger manoeuvre time. Retaining higher sloshing modes has a major effect on the free-surface motion compared to the swing motion. In addition to making the response slower, suppressing residual oscillations at higher sloshing modes has a minor improvement. The total manoeuvre times for a single, three, five, and seven sloshing modes are 3.27, 3.35, 3.29, and 3.45 s, respectively. Using three to five sloshing modes is quite sufficient in representing the liquid sloshing dynamics.

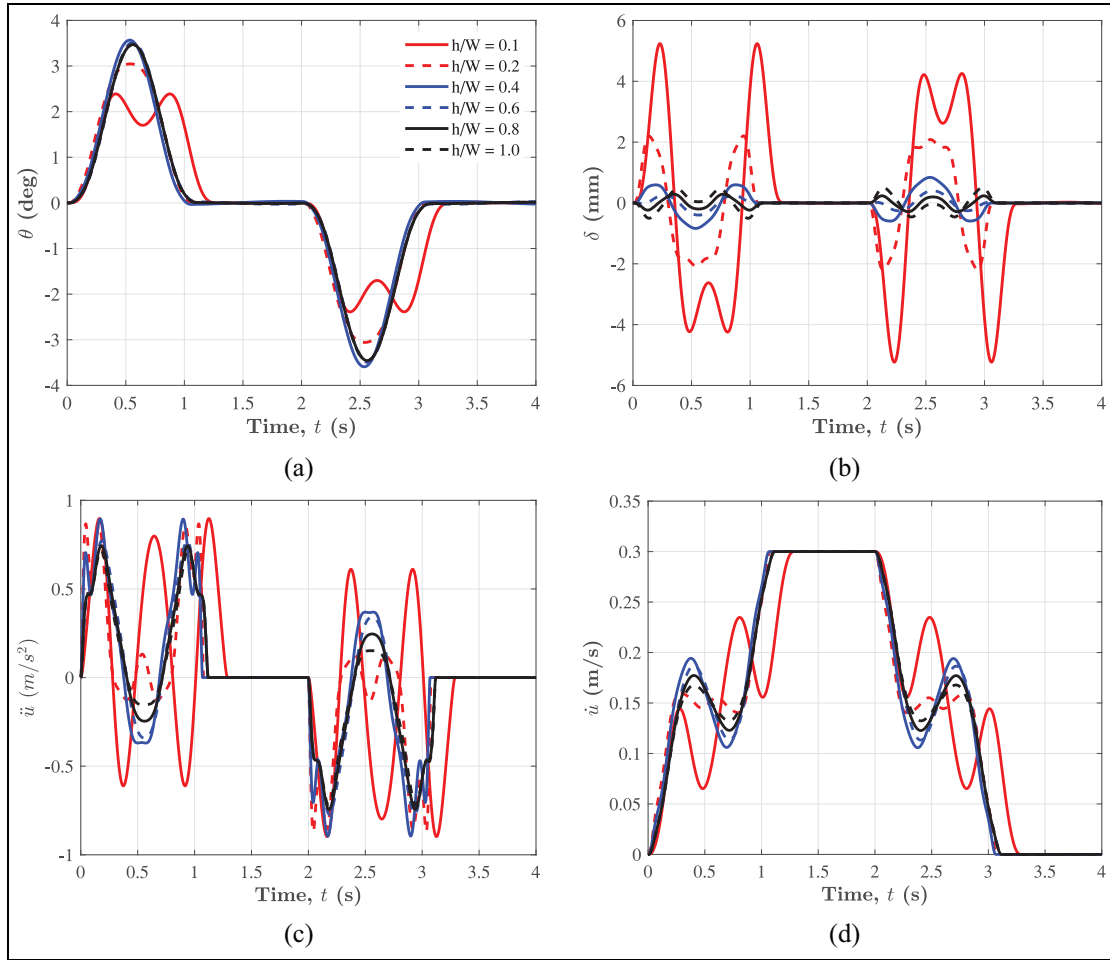


Figure 7. Smooth PSCs and the corresponding dynamic responses using different liquid depth ratios, h/W ($l/H = 0.6$ and $n = 5$): (a) swing angle; (b) free-surface wave motion; (c) jib acceleration; and (d) jib velocity.

To further assess the effect of sloshing modes in command-designing, the influence of the higher modes in a command designed based on lower modes is illustrated in Figure 6. Figure 6(a) shows the response of higher sloshing modes, $n = 3, 5$, and 7 subjected to a smooth PSC designed based on a single mode, $n = 1$ (seven coefficients). Figures 6(b) to 6(d) show the response of higher sloshing modes when subjected to smooth PSCs designed using lower modes. It is clear that designing a smooth PSC based on five modes, $n = 5$, will guarantee the elimination of the residual vibrations from the higher modes.

Variation of liquid depth. The sloshing frequencies depend on the liquid-filling level to the width of the container, h/W . Using five sloshing modes and cable length ratio of $l/H = 0.6$, the smooth PSC and its corresponding dynamics response are depicted in Figure 7. The wave surface oscillations decrease with the increasing of the liquid level. The dynamic response and the input profile of a shallow water depth $h/W = 0.1$ are quite different than the responses of deep water depths, $h/W \geq 0.2$. As shown in Figure 7(a), the

swing angle experiences two peaks due to the liquid sloshing in the acceleration (and deceleration) stage. The motion of the liquid free-surface was significantly reduced (see Figure 7(b)), and the maximum swing angle was slightly increased (see Figure 7(a)), with the increasing of the liquid depth, that is, increasing the mass of the liquid. The PSC, and hence the dynamic response, of the liquid container with $h/W \geq 0.4$ are almost identical. If the liquid depth exceeds a certain critical value, the sloshing frequencies do not significantly change. Therefore, a controlling technique has to be employed in conveying a shallow liquid-filled container with $h/W \leq 0.2$.

Variation of cable length. The frequency corresponding to the swing motion depends on the length of the cable, l , that attaches the container to the moving jib. Using five sloshing modes and a liquid depth ratio of $h/W = 0.1$, the smooth PSC and its dynamics response are illustrated in Figure 8 when using different cable lengths. The increase in the cable length increases the manoeuvre time and induces larger liquid-surface oscillations. The dynamic responses and input profiles of the suspended system with a long cable length

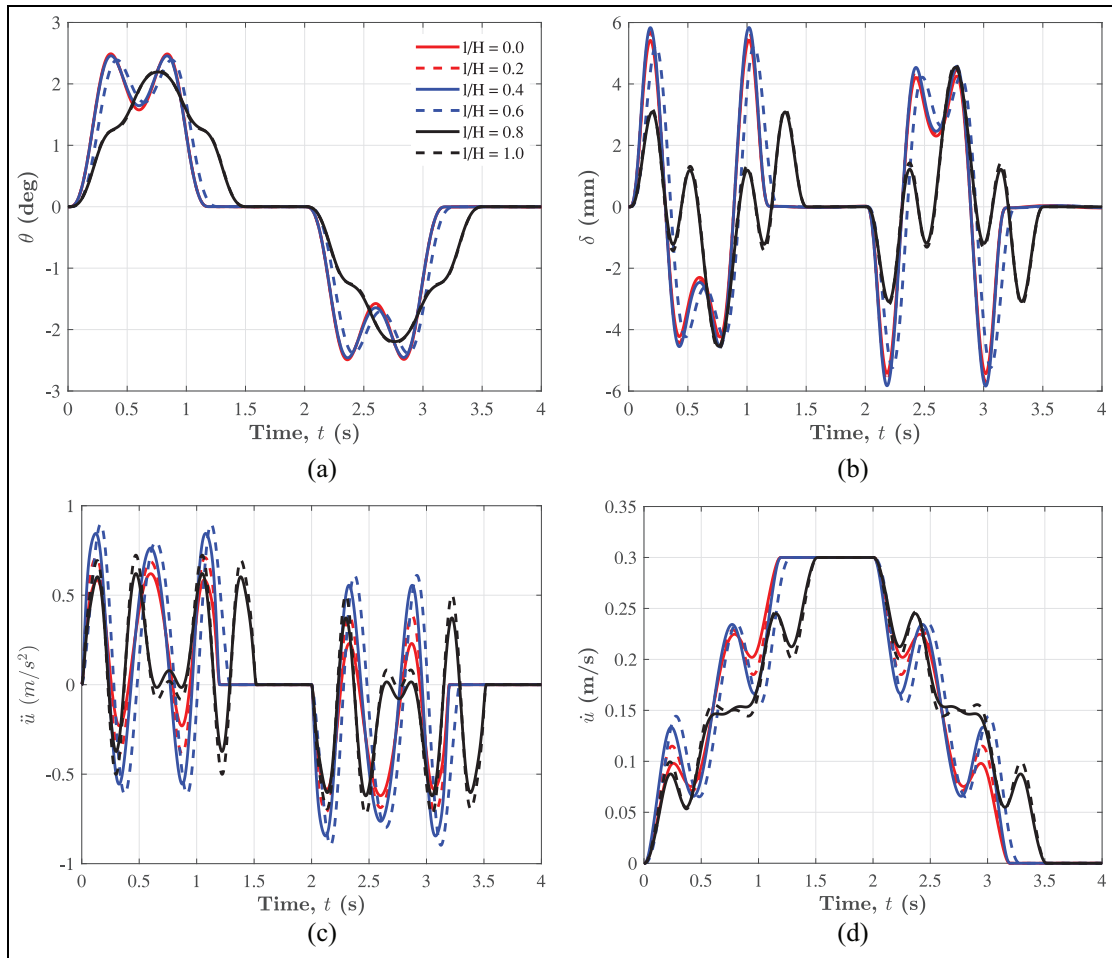


Figure 8. Smooth PSCs and the corresponding dynamic responses using different cable length ratios, l/H ($h/W = 0.1$ and $n = 5$): (a) swing angle; (b) free-surface wave motion; (c) jib acceleration; and (d) jib velocity.

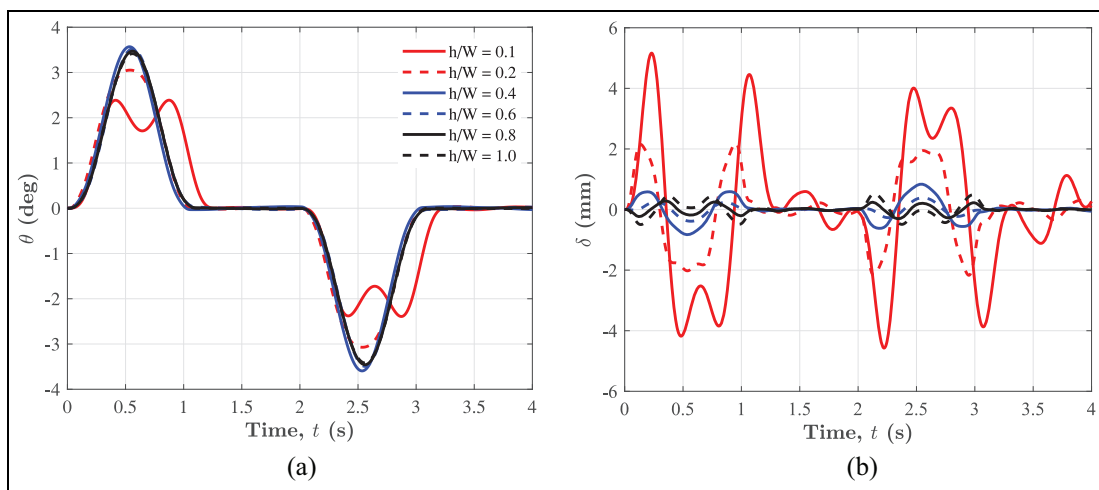


Figure 9. The effects of introducing damping ($\zeta = 0.01$) on the dynamic responses for different liquid depth ratios ($l/H = 0.6$ and $n = 5$): (a) swing angle; and (b) free-surface wave motion.

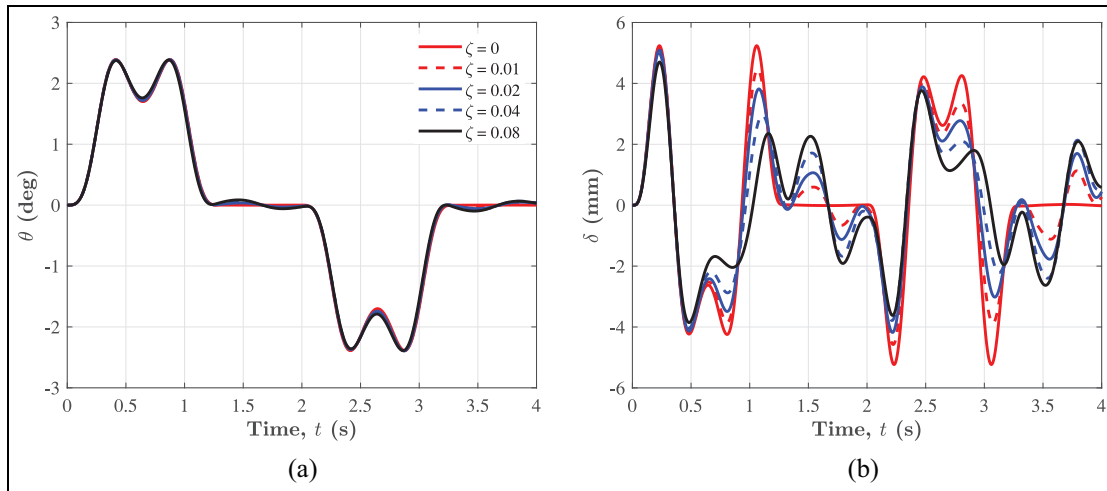


Figure 10. The effects of adding damping on the dynamic responses ($h/W = 0.1$, $l/H = 0.6$, and $n = 5$): (a) swing angle; and (b) free-surface wave motion.

$l/H \geq 0.6$ are quite different than the responses of the system with a short cable length, $l/H < 0.6$. The PSCs, and hence the dynamics responses, of the liquid container with $l/H \leq 0.6$ are almost identical. This suggests that the PSC is sensitive to the changes of the cable length.

Effects of introducing damping. The previous analyses were performed while neglecting the effect of the dissipative force of the water on the container's wall. The water damping ratio can be taken as $\zeta = 0.01$ based on the approximation of an analytical expression given in Abramson (1966). For the smooth PSC designed for the undamped system and based on five sloshing modes and a cable length ratio of $l/H = 0.6$, the effects of introducing damping on the dynamic responses, swing angle and free-surface wave motion, for different depth ratios are illustrated in Figure 9. It is clear from Figure 9 that the damping has negligible effects on deep water depths, $h/W \geq 0.4$. However, for shallow water depths, $h/W \leq 0.2$, the residual sloshing is not completely suppressed in the cruising stage. To further assess the effects of adding more damping on a shallow water depth ($h/W = 0.1$), the dynamic responses for different damping ratios are depicted in Figure 10. Adding more damping will increase the residual sloshing in the cruising stage where no noticeable change is observed in the swing angle.

Sensitivity analysis

The PSC is designed based on the actual system's resonant frequencies. These frequencies are usually approximate values determined either experimentally or from a dynamics model. Therefore, variations in one or more frequencies due to the changes in the liquid depths during manoeuvre and/or the measuring uncertainty in the cable length and liquid depth will certainly produce nonzero residual oscillations at the end of the manoeuvre. Hence, it is necessary to test the robustness of the PSC designed based on certain system parameter

values by applying it to a model with different parameter values. The vibration amplitude at the end of the command duration is computed as given by Equation (25):

$$\text{Vib.Amp.} = \sqrt{\theta(t_a)^2 + \left(\frac{\dot{\theta}(t_a)}{\omega_{n,1}}\right)^2} + \frac{1}{h} \sum_{i=1}^n \sqrt{q_i(t_a)^2 + \left(\frac{\dot{q}_i(t_a)}{\omega_{n,i+1}}\right)^2} \quad (25)$$

The percentage of the vibration amplitude of the PSCs to the vibration amplitude of the TORB command versus the changes of the liquid depth and cable length are illustrated in Figure 11. The shaded regions in Figure 11 represent the 5% vibration tolerance.

For instance, using the determined coefficients from a cable length of 0.3 m and a water depth of $h_m = 25$ mm ($h/W = 0.1$), the numerically simulated vibration amplitude percentage when varying the water depth $\pm 30\%$ from its nominal depth is plotted in Figure 11(a) using different command lengths. The PSC is clearly sensitive to the changes of the water depth in shallow water depths. The command robustness is enhanced when using larger command lengths. If the analysis was repeated for a water depth ratio of $h/W = 0.2$, the PSC becomes less sensitive to the depth changes (see Figure 11(c)). The same behaviour can be observed for a water depth ratio of 0.4 (see Figure 11(e)). Consequently, a PSC is expected to give superior performance when the operating depth is larger than the designed modelled depth.

The computed vibration amplitude percentages when changing the cable length $\pm 50\%$ from its nominal length, $l_m = 0.3$ m, are plotted in Figures 11(b), 11(d), and 11(f) for different water depth ratios and command lengths. Similarly, increasing command length will increase the command robustness. Furthermore, Figures 11(b), 11(d), and 11(f) also suggest that PSC becomes less sensitive to the changes of the cable length in deep water depths.

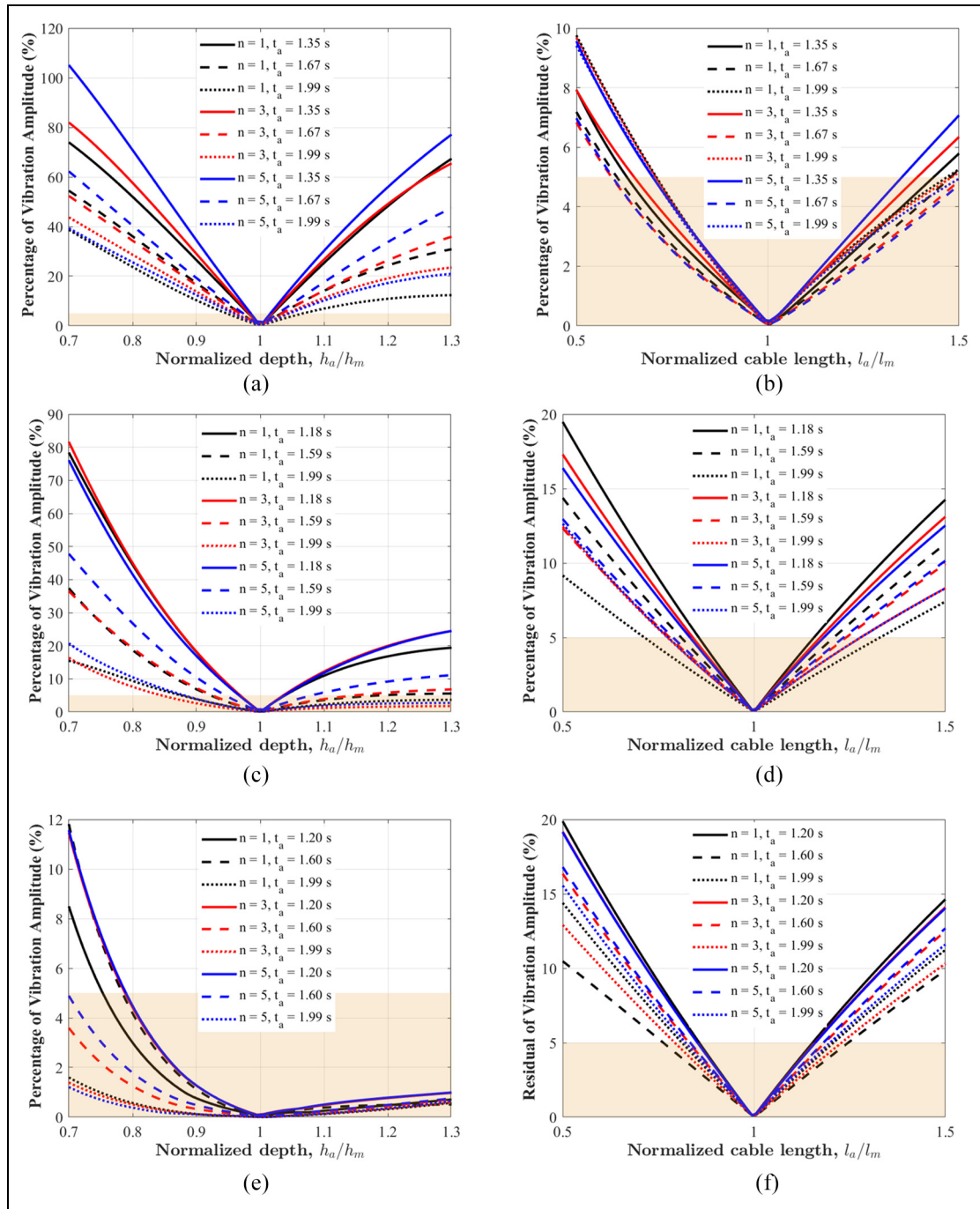


Figure 11. Sensitivity analysis of the proposed PSC to the changes of liquid depth and cable length for different sloshing modes, n , and command length, t_a : (a) $h/W = 0.1$; $h_m = 25$ mm and $l = 0.3$ m; (b) $h/W = 0.1$; $h = 25$ mm and $l_m = 0.3$ m; (c) $h/W = 0.2$; $h_m = 50$ mm and $l = 0.3$ m; (d) $h/W = 0.2$; $h = 50$ mm and $l_m = 0.3$ m; (e) $h/W = 0.4$; $h_m = 100$ mm and $l = 0.3$ m; and (f) $h/W = 0.4$; $h = 100$ mm and $l_m = 0.3$ m.

The time-varying of the water depth, the estimate design values of the cable length and water depth, and the nonlinearities of the system do not guarantee zero residual vibrations in the actual system. Therefore, command robustness can be improved by several ways. Increasing the command interval

enhances the command robustness as shown in Figure 11. In addition, the robustness could also be enhanced by using a higher order polynomial, with coefficients more than the minimum number $m = 2n + 2$ required to satisfy the rest-to-rest manoeuvres, and using the excess to enhance the command

robustness. In addition, two fictitious frequencies could be added adjacent to the modelling frequency (analogous to the extra-insensitive technique) to widen the range of command robustness. Finally, and similar to the concept of zero-vibration-derivative shaper, adding extra constraints of setting the derivative of the residual vibration amplitude with respect to natural frequencies to zero also improves the command robustness. To limit the maximum free-surface sloshing during the motion, an appropriate command length should be chosen accordingly or an additional constraint that limits the maximum water elevation to within a certain predefined value could be imposed in the command-designing process.

Conclusions

A smooth PSC which can be designed from the system's natural frequencies and damping ratios was proposed for eliminating the residual vibrations of a multi-mode system without the full knowledge of the system model. The independence of the command's time length suggests unlimited possibilities of optimum profiles that compensate between the manoeuvre time (speed), transient deflection (safety), input power (energy), etc. However, there is a minimum command length governed by the maximum allowable command amplitude. The continuous form of the proposed PSC renders the possibility of adjusting any level of smoothness, eliminates jerks, that is, inrush currents, enhances actuator's performance and eliminates the inaccurate timing and delay of the actuator.

The efficacy of the PSC is demonstrated by suppressing the liquid sloshing of a suspended liquid container. The proposed model accounts for the coupling between the pendulum dynamics and the sloshing dynamics represented by an equivalent mechanical model that is based on a series of mass-spring-damper systems. Even though the PSC slowed down the system compared to the uncontrolled command, the reduction of the liquid oscillations during the overall motion was significant. The effectiveness of the PSC with variations in the system and command-designing parameters was demonstrated using numerical simulations. At least five sloshing modes should be considered when modelling the sloshing dynamics. Parametric sensitivity analyses are conducted to test the robustness of the PSC over a wide range values of cable length and liquid depth. The results suggest using an understated water depth when designing the PSC. The time interval of the command should be selected to compensate between the operational time, desired transient reduction, and command's sensitivity. For a container subjected to a higher speed, the nonlinear model should alternatively be used in command-designing.

It should be noted that the PSC can be designed for any set of driven-motor capabilities (d , v_f , and a_{\max}) and system parameters ($\omega_{n,i}$ and ζ_i represented by the container dimension and the inside fluid). Therefore for a real case situation, these values are changed and a PSC can be designed accordingly. The presented results show the effectiveness of the PSC when employing higher sloshing modes, changing liquid depth and cable length, and introducing water damping effects. It is necessary to employ a controlled input when conveying shallow water depth containers.

Acknowledgement

The authors would like to thank Dr. Mohammed Alfares at Kuwait University.

Declaration of conflicting interests

The authors declared no potential conflicts of interest with respect to the research, authorship, and/or publication of this article.


Funding

The authors received no financial support for the research, authorship, and/or publication of this article.

Note

1. To avoid confusion, masses and spring constants are always denoted by the symbols m_i and k_i , respectively, with lower subscript.

ORCID iD

Abdullah Alshaya  <https://orcid.org/0000-0002-9105-5300>

References

- Abuel-Hassan A, Arafa M and Nassef A (2009) Design and optimization of input shapers for liquid slosh suppression. *Journal of Sound and Vibration* 320(1): 1–15.
- Abramson HN (ed.) (1966) *The Dynamic Behavior of Liquids in Moving Containers, with Applications to Space Vehicle Technology*. National Aeronautics and Space Administration Technical Report SP-106. Available at: <https://ntrs.nasa.gov/archive/nasa/casi.ntrs.nasa.gov/19670006555.pdf> (accessed 28 August 2019).
- Alghanim KA, Majeed MA and Alhazza KA (2018) Adjustable-smooth polynomial command-shaping control with linear hoisting. *Journal of Vibration and Acoustics* 140(061013).
- Alhazza KA and Masoud ZN (2016) Waveform command shaping control of multimode systems. *Journal of Sound and Vibration* 363: 126–140.
- AlSaibie A and Singhose W (2013) Experimental testing of liquid slosh suppression in a suspended container with compound-pendulum dynamics. In: *9th Asian Control Conference (ASCC)*, Istanbul, Turkey, 23–26 June 2013. Piscataway, NJ: Institute of Electrical and Electronics Engineers, 1–6.
- Alshaya A and Alghanim K (in press) Command-Shaping for Sloshing Suppression of a Suspended Liquid Container. *Journal of Dynamic Systems, Measurement and Control*. Epub ahead of print. DOI: 10.1115/1.4047957.
- AlSaibie A and Singhose W (2013) Experimental testing of liquid slosh suppression in a suspended container with compound-pendulum dynamics. In: *9th Asian Control Conference (ASCC)*, Istanbul, Turkey, 23–26 June 2013. Piscataway, NJ: Institute of Electrical and Electronics Engineers, 1–6.
- Baozeng Y and Lemei Z (2014) Hybrid control of liquid-filled spacecraft maneuvers by dynamic inversion and input shaping. *AIAA Journal* 52(3): 618–626.
- Biagiotti L, Chiaravalli D, Moriello L, et al. (2018) A plug-in feed-forward control for sloshing suppression in robotic teleoperation tasks. In: *2018 IEEE/RSJ International Conference on Intelligent Robots and Systems (IROS)*, Madrid, Spain, 1–5 October 2018.

- Piscataway, NJ: Institute of Electrical and Electronics Engineers, 5855–5860.
- Cooker MJ (1994) Water waves in a suspended container. *Wave Motion* 20(4): 385–395.
- Feddema JT, Dohrmann CR, Parker GG, et al. (1997) Control for slosh-free motion of an open container. *IEEE Control Systems Magazine* 17(1): 29–36.
- Graham E and Rodriguez A (1952) Characteristics of fuel motion which affect air plane dynamics. *Journal of Applied Mechanics* 19: 381–388.
- Hasheminejad SM, Mohammadi M and Jarrahi M (2014) Liquid sloshing in partly-filled laterally-excited circular tanks equipped with baffles. *Journal of Fluids and Structures* 44: 97–114.
- Huang J and Zhao X (2018) Control of three-dimensional nonlinear slosh in moving rectangular containers. *Journal of Dynamic Systems, Measurement, and Control* 140(081016).
- Hyde J and Seering M (1991) Using input command pre-shaping to suppress multiple mode vibration. In: *Proceedings 1991 IEEE International Conference on Robotics and Automation*, Vol. 3, Sacramento, California, USA, 9–11 April 1991. Piscataway, NJ: Institute of Electrical and Electronics Engineers, 2604–2609.
- Ibrahim RA (2005) *Liquid Sloshing Dynamics: Theory and Applications*. 1st edition. New York: Cambridge University Press.
- Kaneshige A, Kaneshige N, Hasegawa S, et al. (2008) Model and control system for 3d transfer of liquid tank with overhead crane considering suppression of liquid vibration. *International Journal of Cast Metals Research* 21(1): 293–298.
- Kaneshige A, Kitaoka T, Munetoshi H, et al. (1997) Motion control of an overhead travelling crane with hoisting motion and curve trajectory. *Transactions of the Japan Society of Mechanical Engineers Series C* 63(607): 921–928.
- Kaneshige A, Miyoshi T and Terashima K (2009) The development of an autonomous mobile overhead crane system for the liquid tank transfer. In: *2009 IEEE/ASME International Conference on Advanced Intelligent Mechatronics*, Singapore, 14–17 July 2009. Piscataway, NJ: Institute of Electrical and Electronics Engineers, 630–635.
- Kaneshige A, Nishida M and Terashima K (1996) Motion control of a liquid-container crane system considering the suppression of sloshing and the tracking property. *Transactions of the Japan Society of Mechanical Engineers Series C* 62(596): 1321–1328.
- Masoud ZN and Alhazza KA (2017) A smooth multimode waveform command shaping control with selectable command length. *Journal of Sound and Vibration* 397: 1–16.
- Murthy AS, Kivila A and Singhose W (2012) Slosh suppression of a liquid in a suspended container using robust input shaping. In: *19th International Congress on Sound and Vibration*, Vilnius, Lithuania, 8–12 July 2012, pp. 1–8. Available at: http://singhose.marc.gatech.edu/courses/me6404/Past%20Projects/2012_ICSV_CraneSlosh.pdf.
- Pridgen B, Bai K and Singhose W (2013) Shaping container motion for multimode and robust slosh suppression. *Journal of Spacecraft and Rockets* 50(2): 440–448.
- Reyhanoglu M and Rubio Hervas J (2013) Nonlinear modeling and control of slosh in liquid container transfer via a PPR robot. *Communications in Nonlinear Science and Numerical Simulation* 18(6): 1481–1490.
- Singer NC and Seering WP (1990) Preshaping command inputs to reduce system vibration. *Journal of Dynamic Systems, Measurement, and Control* 112(1): 76–82.
- Singer NC and Seering WP (1992) An extension of command shaping methods for controlling residual vibration using frequency sampling. In: *Proceedings 1992 IEEE International Conference on Robotics and Automation*, Vol. 1, Nice, France, 12–14 May 1992. Piscataway, NJ: Institute of Electrical and Electronics Engineers, 800–805.
- Singhose W and Pao L (1997) A comparison of input shaping and time-optimal flexible-body control. *Control Engineering Practice* 5(4): 459–467.
- Singhose W, Seering W and Singer N (1994) Residual vibration reduction using vector diagrams to generate shaped inputs. *Journal of Mechanical Design* 116(2): 654–659.
- Singhose W, Seering WP and Singer NC (1996) Input shaping for vibration reduction with specified insensitivity to modeling errors. In: *Proceedings of the 1996 Japan–USA Symposium on Flexible Automation*, Boston, Massachusetts, 7–10 July 1996, pp. 307–313. New York: American Society of Mechanical Engineers.
- Turner MR and Bridges TJ (2013) Nonlinear energy transfer between fluid sloshing and vessel motion. *Journal of Fluid Mechanics* 719: 606–636.
- Turner M, Alemi Ardakani H and Bridges T (2015a) Instability of sloshing motion in a vessel undergoing pivoted oscillations. *Journal of Fluids and Structures* 52: 166–180.
- Turner M, Bridges T and Alemi Ardakani H (2015b) The pendulum-slosh problem: Simulation using a time-dependent conformal mapping. *Journal of Fluids and Structures* 59: 202–223.
- Wang W, Peng Y, Zhou Y, et al. (2016) Liquid sloshing in partly-filled laterally-excited cylindrical tanks equipped with multi baffles. *Applied Ocean Research* 59: 543–563.
- Xing B and Huang J (2020) Control of pendulum-sloshing dynamics in suspended liquid containers. *IEEE Transactions on Industrial Electronics* 99: 1–1. Epub ahead of print 7 May 2020. DOI: 10.1109/TIE.2020.2991933.
- Yano K and Terashima K (2001) Robust liquid container transfer control for complete sloshing suppression. *IEEE Transactions on Control Systems Technology* 9(3): 483–493.
- Zang Q and Huang J (2015) Dynamics and control of three-dimensional slosh in a moving rectangular liquid container undergoing planar excitations. *IEEE Transactions on Industrial Electronics* 62(4): 2309–2318.
- Zang Q, Huang J and Liang Z (2015) Slosh suppression for infinite modes in a moving liquid container. *IEEE/ASME Transactions on Mechatronics* 20(1): 217–225.

Appendix

Equivalent mechanical model parameters

The equivalent mass m_i , stiffness constant k_i , and viscous damper constant c_i of the i th sloshing mode, the rigid mass m_0 and mass moment of inertia I_0 of the fixed liquid that moves with the container, the distances h_0 and h_i from the liquid's centre of gravity, $h/2$, to the fixed mass m_0 and i th mass point m_i for a two-dimensional rectangular rigid-walled container of width W (in the direction of wave motion) and height H with a liquid filling level h as shown in Figure 1(b) are given by Graham and Rodriguez (1952; Equations (26a) to (26i)):

$$m_i = \frac{8m_f \tanh((2i-1)\pi h/W)}{\pi^3 (2i-1)^3 h/W} \quad (26a)$$

$$\frac{h_i}{h} = \frac{1}{2} - \frac{\tanh((2i-1)\pi h/2W)}{(2i-1)\pi h/2W} \quad (26b)$$

$$k_i = 8m_f g \frac{\tanh^2((2i-1)\pi h/W)}{\pi^2 (2i-1)^2 h} \quad (26c)$$

$$c_i = 2\zeta\omega_i m_i \quad (26d)$$

$$\omega_i = \sqrt{\frac{k_i}{m_i}} = \sqrt{\frac{\pi g}{W} (2i-1) \tanh\left((2i-1)\frac{\pi h}{W}\right)} \quad (26e)$$

$$m_0 = m_f - \sum_{i=1}^n m_i \quad (26f)$$

$$h_0 = -\frac{1}{m_0} \sum_{i=1}^n m_i h_i \quad (26g)$$

$$I_0 = I_F - m_0 h_0^2 - \sum_{i=1}^n m_i h_i^2 \quad (26h)$$

$$I_F = \frac{m_f}{12} \left[h^2 - 3W^2 + \frac{768W^3}{\pi^5 h} \sum_{i=1}^n \frac{\tanh((2i-1)\pi h/2W)}{(2i-1)^5} \right] \quad (26i)$$

where $m_f = \rho Wh = \sum_{i=1}^n m_i$ is the total liquid mass in the container; ω_i corresponds to the natural frequency of the i th sloshing mode of a liquid surface; ζ is the liquid damping ratio; ρ is the liquid density; and g is the gravitational acceleration.

Nomenclature

$\mathbf{a} = a_k$	Polynomial coefficients of the PSC, $\ddot{u}(t)$
a_{\max}	Jib maximum acceleration
\mathbf{B}	Forcing vector
c_i	Equivalent viscous damper constant of the i th sloshing mode
$\mathbf{c} = c_i$	Modal damping matrix
\mathbf{C}	Damping matrix
d	Travel distance
$f(t)$	System input
g	Gravitational acceleration, $g = 9.81 \text{ m/s}^2$
h	Liquid filling level
h_0	Distance from liquid centre of gravity, $h/2$, to the liquid rigid mass, m_0
h_i	Distance from liquid centre of gravity, $h/2$, to the equivalent i th mass point, m_i
H	Container height
I_0	Mass moment of inertia of the liquid rigid mass, m_0
I_c	Mass moment of inertia of the container
I_{eq}	Equivalent mass moment of inertia
k_i	Equivalent spring stiffness constant of the i th sloshing mode
$\mathbf{k} = k_i$	Modal stiffness matrix
\mathbf{K}	Stiffness matrix

l	Length of the rigid link
l_0	Distance from the jib to the liquid fixed-mass, m_0
l_c	Distance from the jib to the container's centre of mass
l_i	Distance from the jib to the i -th lumped mass, m_i
m	Polynomial order of the input shaped command
m_0	Rigid mass of the fixed liquid
m_c	Mass of the container
$\mathbf{m} = m_i$	Modal inertia matrix
m_i	Equivalent mass of the i th sloshing mode
m_f	Total liquid mass, m_f
\mathbf{M}	Inertia matrix
n	Number of liquid sloshing modes
$\mathbf{p} = p_i$	Forcing vector in the modal system
$q_i(t)$	Lateral displacement of the lumped mass m_i , that is, surface wave oscillation
\dot{q}_i, \ddot{q}_i	Lateral velocity and acceleration of the lumped mass m_i
Q	Root-mean-square of liquid wave oscillation
s_a, s_c, s_d	Travelled distance in acceleration, cruising, and deceleration stages
t	Time coordinate
t_a, t_c, t_d	Time interval of acceleration, cruising, and deceleration stages
T	Total manoeuvre time
u, \dot{u}, \ddot{u}	Jib horizontal displacement, velocity, and acceleration
v_f	Jib maximum velocity
W	Container width
$\delta(t)$	Sum of the lateral displacements of the lumped masses
ζ	Liquid damping ratio
$\eta(x, y, t)$	Free-surface liquid elevation
$\theta(t)$	Swinging angle in xy -plane measured clockwise from vertical y -direction
$\dot{\theta}, \ddot{\theta}$	Angular velocity and acceleration
Θ	Vector of generalized coordinates, $\Theta = \theta q_1 \cdots q_n^T$
ρ	Liquid density
τ	Command length
ϕ_i	Spatial sloshing mode
Φ_i	Mode shape
Φ	Modal matrix
$\Psi = \psi_i$	Vector of principal (decoupled) coordinates
ω_i	Natural frequency of the i th sloshing mode
$\omega_{n,i}, \omega_{d,i}$	Undamped and damped natural frequencies
$(\dot{\quad})$	Time derivative, d/dt